Formation of Aligned Microfiber Arrays via Self-Assembling SiO_2 Nanocolloids. Change of Microfiber Structure during Annealing

Valery Shklover*

Laboratory of Crystallography, Swiss Federal Institute of Technology, CH-8092 Zürich, Switzerland

Received July 12, 2004. Revised Manuscript Received November 1, 2004

Self-assembling spherical colloidal SiO_2 nanoparticles using shear flow leads to the formation of the films, consisting of aligned one-layer microfibers. The termination of fabricated microfibers and films can be described in terms of crystallographic faces of corresponding close-packed structures, which in turn are preset by the kinetic conditions of crystallization. An in-situ X-ray study of the transformation of the nanocrystalline microfibers at high-temperature into a mixture of silica polymorphs with the high-temperature β-cristobalite and tridimite as major components is performed. Microfibers heated in the middle temperature zone exhibit graded morphology, with the degree of coalescence of amorphous nanoparticles changing along the microfiber length. The performed study can be considered as a part of the development of a strategy (which could require both self-assembly and template-assisted steps) toward a bottom-up approach to the design of nanostructure arrays for technological applications.

Introduction

Self-assembly is an efficient approach of nanotechnology for the design of ordered nano- and micrometer ensembles. In this paper, we describe how from self-assembling nanoparticles, micrometer-sized, low-dimensional crystalline arrays can be obtained with predictable crystallographic orientation with regards to the crystallization environment. Ordered nano- and microcrystalline arrays leave room for new opportunities and secure properties, critical for the function of corresponding devices such as directional heat transport from miniature semiconductor devices (or biological systems) or tuning photonic band gap structure.

Controlled heat treatment is one of the a posteriori treatments aimed at stabilization of self-assembled arrays. However, heat treatment (sintering) can change the nanocrystalline nature of the nanoarray. Studies of controlled heat treatment provide information about many properties of nanocrystalline materials such as (a) the dependence of densification on the degree of agglomeration and primary nanoparticle size, (b) the possibility of densification without an explosive grain growth, (c) the possibility of sintering nanopowder at the temperature lower than those for micrometer-sized powders, (d) the possible influence of the presence of a thin film of nanocrystalline oxide on the phase composition of the oxides, thermally grown on metal surfaces, and (e) the influence of the possible presence of amorphous phase and possible strains in the crystalline phase on the crystallization during heat treatment. More promising results with regards to sintering behavior have been achieved by using nanopowders in stable crystallographic form, for example, fully dense nanograin ceramics of ZrO_2.[1−4]

The aims of this work, which was intended as part of a more general study into the use of self-assembling as a step in design of low-dimensional nano- and microcrystalline arrays, were (a) fabrication of macroscopic colloidal arrays using a shear flow self-assembling method, (b) study of the relation between the symmetry of crystallization cell environment and self-assembled arrays, and (c) study of heat treatment of self-assembled nanocolloidal arrays.

Experimental Section

Materials. The 80 nm Klebosol monodisperse colloidal SiO_2 spheres Cat. No. 30R50 (Clariant Corp.) were used for crystallization of nanocrystalline array (NCA1). To estimate the exact particle size distribution, the film of SiO_2 spheres on the 1−2 nm amorphous carbon film was prepared, coated with 2 nm W layer to avoid the charging problem, and examined at 30 kV accelerating voltage in a Hitachi S-900 field-emission SEM with a standard Everhard-Thornley SE detector and a YAG type BSE detector (see Supporting Information). The obtained SEM patterns were studied with analySIS software (Soft Imaging Systems GmbH, Germany). The amorphous character of Klebosol monodisperse colloidal SiO_2 spheres was demonstrated by a TEM study of isolated 50 nm particles (see Supporting Information).

Fabrication of Nanocrystalline Arrays. The method described in ref 5 was used for fabrication of nanocrystalline arrays. The gaskets for the packing cell were constructed form micro slides (Superiors, Marienfeld, Germany) and polyester film with the thickness of $d = 25$, 36, and 50 μm (DuPont Teijin Luxemburg).

* Phone: +41 1 632 37 75. Fax: + 41 1 632 11 33. E-mail: v.shklover@mat.ethz.ch.

(1) Bowen, P.; Carry, C. *Powder Technol*. **2002**, *128*, 248.
(2) Srdic, V. V.; Winterer, M.; Hahn, H. *J. Am. Ceram. Soc*. **2000**, *83*, 729.
(3) Shklover, V.; Bowen, P.; Belaroui, K.; Hofmann, H.; Konter, M. Patent Application WO 03/068673. (ALSTOM Number: B01/241-0). The essence of this patent disclosure is the promotion of the growth of stable α-Al_2O_3 polymorph in the TGO (thermally grown oxide) by thin (ca. 10 μm) precoating of nanocrystalline α-Al_2O_3. This layer promotes the formation of stable α-Al_2O_3 in TGO and decreases the amount of phase transitions and associated volume changes in the TGO during the protected article service. This increases the stability and lifetime of the article.
(4) Eastman, J. A. *J. Appl. Phys*. **1994**, *75*, 770.

10.1021/cm048870t CCC: $30.25
Published on Web 01/08/2005

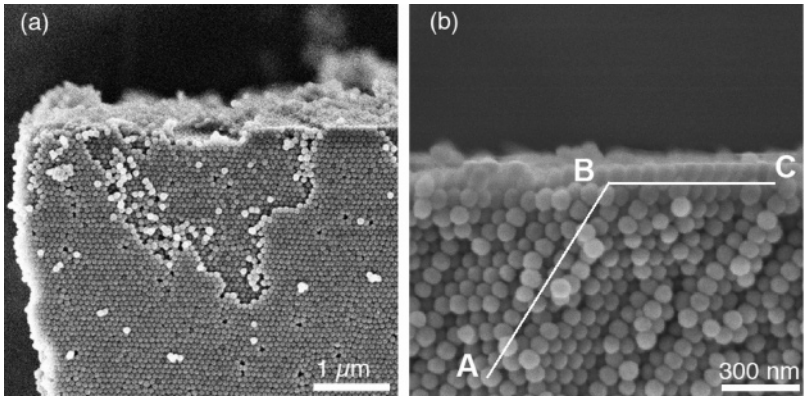

Figure 1. SEM patterns showing ccp structure of microfibers (thickness $d = 36$ μm). (a) Top view along [111]. (b) Side view along [110].

The first of three discussed in ref 5, nonlithographic methods of generation of the channel structure, was applied, the use of a piece of soft paper to wipe the surface of the polyester film. For the crystallization of the colloids, the sonicator Branson 1510 (Bransonic) was operated at a frequency of 42 kHz, maximum power 80 W, RF-power 80 W. The 80 nm Klebosol colloidal silica particles were assembled into colloidal crystals. The first visual and microscopic observations indicated that the formed colloidal film is an array of microfibers with a rectangular cross-section aligned parallel as one layer into a 2D array (film). The thickness of the film was controlled by the thickness of the polyester film used. The fabrication process was continued with interruptions over approximately 5 days. The controlled drying of the samples was done at 90 and 60 °C after the assembly was accomplished.

Scanning Electron Microscopy (SEM). A LEO 1530 microscope with software LEO 32 V02.03 was used (LEO Elektronenmikroskopie GmbH); accelerating voltage was 3 kV, in-lens detector, and samples were coated with 3 nm of Au to avoid charging problems.

Transmission Electron Microscopy (TEM). A Tecnai G^2 F30 microscope with ultrahigh atomic resolution was used (FEI Co., Eindhoven, The Netherlands), operating at an accelerating voltage of 300 kV, was used. The SiO_2 particles were prepared in the mixture of ethanol and acetone and were brought onto the Cu grid, coated with carbon film (Plane GmbH, D-35578 Germany).

Optical Microscopy. A Leica MZ 16 optical microscope in both transmission and reflection modes with software IM 1000 (Leica Microsystems) was used.

X-ray Powder Diffraction. A Mar300 imaging-plate detector system (Marresearch GmbH, 1999), equipped with a house-made furnace,[6] was used for powder diffraction measurements. In this design, the original base of the Mar300 was modified to allow additional translation along the spindle axis to accommodate the furnace. The furnace consists of a housing of stainless steel with integrated water cooling, X-ray entry and exit windows (Kapton), and a window for in-situ observation of the specimen through an external CCD-camera (see Supporting Information). The furnace is filled with helium to provide an inert atmosphere and good thermal stability. Calibration of the furnace in the range from room temperature to 900 °C was performed before the measurements. The quartz-glass capillary, with 0.5 mm diameter and 0.01 mm wall thickness, was filled up to ca. 30 mm length with microfibers and sealed in the air. The sample was rotated in the range of $\phi = 0-180°$ during data collection, 1800 s per exposition with λ(Mo Kα1) = 0.7093 Å (quartz monochromator), collimator diameter of 0.5 mm, and sample to detector distance of 200 mm. The measurement of standard Si sample was performed for precise determination of the sample to detector distance and *x*,*y*-pixel coordinates of the direct beam. The measurements at 20, 200, 400, 500, 550, 600, 700, 750, 800, 850, 900, 950 (20 successive measurements were performed at this temperature), 800, 500, and 20 °C were performed; the heating/cooling rate was 10 °C/min, and the holding time at each predetermined temperature was equal to the duration of the X-ray exposition (30 min). All of the X-ray experiments on Mar300 were performed using the mar345(dtb) software package (Marresearch GmbH, 2003); the conversion of X-ray results from 2D to 1D data was done with FIT2D software.[7] The XRS-82 software package[8] was used for treatment of powder diffraction data. The STOE automated powder diffractometer system was used to check the phase composition of the microfibers, treated in the "cold" part of the capillary during the annealing (Debye−Scherrer scan mode, Cu Kα, Ge(111) monochromator, a linear position sensitive detector).

Results and Discussion

The examination of the SEM patterns (Figure 1) clearly indicates the hexagonal packing of the SiO_2 spheres in microfibers, the ...ABC... stacking sequence of layers of silica beads, and the resulting ccp structure (space group $Fm\bar{3}m$, packing density 0.74), observed in many colloidal crystals.[9] The structure of the microfibers, built of the not-perfect monodisperse SiO_2 nanoparticles (see Supporting Information), has many defects. The disordered structure of the nanoarray seems to be problematic for photonic and microelectronic applications.

The main approaches to organization of nanostructures into unidirectional arrays are discussed in review[10] and can be divided into the following:

(a) The first is crystallization of materials possessing intrinsic highly anisotropic crystal structure. (The crystallization of trigonal PbI_2 into trigonal nanocrystals of 5−10 nm size and then into trigonal assembles of 100−300 nm size[11] is another example of conservation of the intrinsic unit

(5) Xia, Y.; Gates, B.; Yin, Y.; Lu, Y. *Adv. Mater*. **2000**, *12*, 693.
(6) Estermann, M.; Reifler, H.; Steurer, W.; Filser, F.; Kocher, P.; Gauckler, L. *J. Appl. Crystallogr*. **1999**, *32*, 833.
(7) Hammersley, A. P. FIT2D V10.3 Reference Manual V4.0, ESRF98HA01T, ESRF, August 26, 1998.
(8) Baerlocher, Ch. XRS-82. The X-ray Rietveld System, Institut für Kristallographie, ETH, Zurich, Switzerland, 1982.
(9) Xia, Y.; Gates, B.; Park, S. H. *J. Lightwave Technol*. **1999**, *17*, 1956.
(10) Xia, Y.; Yang, P.; Sun, Y.; Wu, Y.; Mayers, B.; Gates, B.; Yin, Y.; Kim, F.; Yan, H. *Adv. Mater*. **2003**, *15*, 353.
(11) Shklover, V.; Grätzel, M. *Org.−Inorg. Hybrid Mater. Photonics Proc. SPIE* **1998**, *3469*, 134.

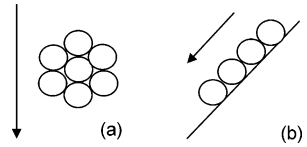

Figure 2. Preferential crystallographic orientation of colloidal array imposed by growth conditions. (a) One of the crystallographic directions of the nanoarray of spherical particles oriented preferentially along the streamline of the shear flow cell. (b) Template geometry dictates crystallographic orientation of the external top and bottom faces of the nanoarray parallel to the substrate. Arrows indicate direction of the streamline of the shear flow, which is very slow and comparable to the sedimentation rate. The possibility of controlling kinetically the crystallographic orientation of the nanoarray is beneficial for practical applications.

cell shape into the shape of the nanocrystalline aggregate during crystal growth.)

(b) The second is template-directed synthesis and generic approaches (use of the symmetry of the environment) for crystallization of materials with isotropic crystal structure.

The observed ccp structure of microfibers is one of the examples of highly anisotropic growth as a result of symmetry of the environment. If a crystal, which belongs to a high symmetry system, grows in a limited space where the materials to be deposited are supplied unidirectionally (flow, diffusion, convection), distorted highly anisotropic crystals can be formed.[12]

Shear-flow crystallization is a convenient assembling method, but its understanding requires the account of several complex processes: (a) sedimentation in a gravitational field, (b) hydrodynamic shear-flow with very small velocity, (c) Brownian motion and particles diffusion, (d) local fluctuations caused by ultrasonic sound waves radiation, and (e) capillary stresses (can lead to cracking the film during the drying). At the crystallization level, the formation of microfibers can be considered as the result of a combination of the preferential growth mechanism of the primary nanocrystallites (small arrays formed by several primary nanoparticles) and geometrical constraints imposed by geometry of crystallization cell. The rational crystallographic orientation of the faces of the microfibers with regards to the crystallization cell draws attention. One of the crystallographic directions of microfibers is along the streamline of the shear flow, while the second one is parallel to the template surfaces, Figure 2. This means that we can use the shear flow direction and template geometry for the control of the array crystallography. This is beneficial for practical applications. The parallel assembling of nanowires (NW) and nanotubes (NT) on the chemically patterned substrates is another example of the use of fluidic alignment (shear flow) for hierarchical assembly of 1D nanomaterials into a functional network with controlled periodicity and of the several micrometer-size.[13] The dependence of the NW angular distribution on the shear-flow rate was also established.[13]

The similarity of the distribution of the microfiber shapes as compared to the streamlined (velocity distribution) patterns of laminar flow in a water-filled cavity is remarkable. Both have straight streamlines in the middle of the cell and rotating rolls at the corners, with a gradient of microfibers width (stream velocity) directed from the resevoir to the cell walls.[14] This similarity can support the slow drying mechanism of the microfiber formation under the condition of a very slow shear rate that is comparable to the crystallization rate.

All of the microfibers have thickness, prescribed by polyester film thickness d, and a width ranging approximately from ca. 50 to 200 μm. In the central, most homogeneous part of the cell, the straight microfibers can be approximately characterized by dimensions of $d \times 150 \times 10000$ μm, with the long axes of the microfibers approximately parallel to the shear in the homogeneous part of the film, Figure 3. The arrays of aligned microfibers with the largest thickness $d =$ 50 μm exhibit the best quality. The microfibers have remarkable mechanical stability. A possible mechanism of cracking primary 2D array into microfibers can be described by high capillary stresses and counteracting adherence to the substrate.[15] We did not use the previously described methods[15] of drying to avoid cracking that could include supercritical drying, drying with solvent of smaller surface tension, freeze-drying, or slow evaporation. The formation of the microfibers during the drying process and not during the crystallization was proven by detailed observation of the lines pattern on the belts surfaces, Figure 3b. Of course, the microfibers could find an application as mats (both supporting and free-standing),[16] but the observed perfect aligned microfibers with predictable crystallographic orientation could find new practical applications as compared to corresponding unordered structures. The formation of 2D nano- or microarrays with planar or curvature high-density structure is illustrated by Figure 4.

The lithographically designed rectangular microchannels were used by Ozin and co-workers for growth of silica colloidal crystals of different geometries and on different substrates with directed evaporation induced self-assembly (DEISA).[17] It could be seen from the observation of SEM patterns that the crystallization takes place within the channels, indicating that capillary forces were driving the process. The SEM top-view shows the hexagonal packing of the spheres. The spatial coherence along the channels is on the order of hundreds of micrometers, sometimes millimeters. The consideration of the SEM patterns also shows the rational crystallographic orientation of the arrays related to the microchannel walls. This orientation is the result of a complex growth process including capillary, convection, and gravitational forces, as well as particle···particle and particle··· wall interactions. The particles tend to create high-density crystalline surfaces in contact with the flat walls or substrate.

To check the sintering properties, we carried out the high-temperature in-situ X-ray study of the microfibers placed into the quartz capillary of the diameter 0.5 mm and length ca. 30 mm. The X-ray image plate scanner MAR300,

(12) Givargizov, E. I. *Highly Anisotropic Crystals*; D. Reidel Publishing Co.: Dordrecht, The Netherlands, 1987; p 39.
(13) Huang, Y.; Duan, X.; Wei, Q.; Lieber, C. M. *Science* **2001**, *291*, 630.
(14) Lankhorst, A. M. Laminar and Turbulent Natural Convection in Cavities. Ph.D. Thesis, Technische Universiteit Delft, 1991; p 94.
(15) Bellet, D.; Canham, L. *Adv. Mater*. **1998**, *19*, 487.
(16) Li, D.; Wang, Y.; Xia, Y. *Nano Lett*. **2003**, *3*, 1167.
(17) Miguez, H.; Yang, S. M.; Tetreault, N.; Ozin, G. A. *Adv. Mater*. **2002**, *14*, 1805. Yang, S. M.; Miguez, H.; Ozin, G. A. *Adv. Funct. Mater*. **2002**, *12*, 425. Ozin, G. A.; Yang, S. M. *Adv. Funct. Mater*. **2001**, *11*, 95.

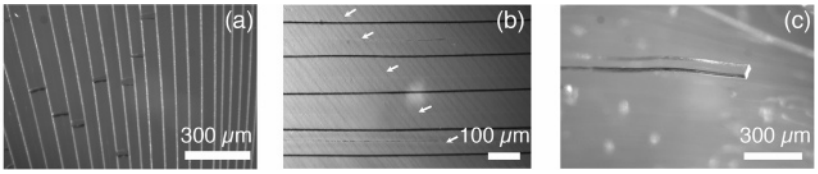

Figure 3. Optical photograph showing morphology of microfibers (thickness $d = 25$ μm) after drying. (a) Photograph recorded in reflectance mode. (b) Photograph recorded in transmission mode. The arrows indicate one of the pattern lines on the surface of microfibers, confirming the cracking of primary 2D array into microfibers during the drying. The observed line pattern on the belt surface could result from the oblique orientation of the packing cell during the crystallization. (c) An isolated microfiber, built of sintered colloidal SiO_2 nanoparticles, can be characterized by dimensions of $25 \times 150 \times 10\,000$ μm and shows remarkable mechanical stability.

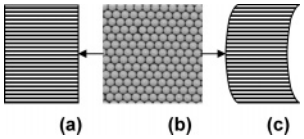

Figure 4. Possible gratings built of patterned arrays of nanocrystalline building blocks (Figure 3a). (a,c) Plane and curvature gratings. (b) Nanocrystalline moiety, constituting, for example, the black lines in (a) and (c).

equipped with the high-temperature furnace, was used (see Supporting Information). The phase changes were checked in situ in the small part of the capillary, which remained in the X-ray beam during the measurements (X-ray spot size of 0.5 mm). Three different zones can be distinguished in the capillary after the heating (Figure 5). In the high-temperature zone, three structure transformations during the annealing can be observed (Figure 6). The colloidal SiO_2 microfibers crystallize into cubic β-cristobalite ($Fd\bar{3}m$, $D_x = 2.186$ g cm^{-3}) between 750 and 800 °C. As a result of continuous heating at 950 °C during 12 h, the β-cristobalite transforms into a mixture of coexisting β-cristobalite (major phase) and hexagonal β-tridymite ($P6_3/mmc$, $D_x = 2.244$ g cm^{-3}). Cooling to room temperature leads to the formation of a product containing β-cristobalite, β-tridymite (major phases), and low quartz. According to ex-situ X-ray study, performed ca. 7 days after annealing, the middle zone of the capillary (Figure 5b) contains a mixture of tetragonal α-cristobalite ($P4_32_12$, $D_x = 2.350$ g cm^{-3}) and monoclininc α-tridimite (Cc, $D_x = 2.269$ g cm^{-3}).

Formation of high-temperature polymorphic modification of SiO_2 cubic β-cristobalite at 750−800 °C during annealing of colloidal crystal draws attention. According to the generally accepted view of silica phase changes, the α-cristobalite is the stable form at room temperature. However, the presence of β-cristobalite after heat treatment was observed in many other studies; see, for example, ref 18. The transition between α- and β-cristobalite is strongly discontinuous, and the precise transition temperature can be altered by the presence of defects, such as stacking faults and chemical impurities. Additionally, there is a hysteresis in the measured value of T_{tr} on heating and cooling.[19] The β-cristobalite is more disordered than α-cristobalite, and its presence in the product of annealing of colloidal nanocrystalline array immediately after heating could be very characteristic. Different models were developed to explain the disordered structure of β-cristobalite, which has to possess unrealistic Si−O−Si bond angles of 180° and Si−O bond lengths of 1.51 Å. A correlation between the domain theories (see, for example, ref 20) or dynamic theories (see, for example, ref 19) of disorder nature and formation of β-cristobalite from nanocrystalline material observed in the present study is of interest.

The crystallization behavior and phase transitions of nanopowders may not follow the traditional phase transition routes. For example, it was shown[21] that, depending on the synthesis route, nanocrystalline ZrO_2 starts to transform into the high-temperature stable tetragonal polymorph at essentially different temperatures: at ca. 1200 °C for monoclinic crystalline ZrO_2 powder (size of cube-shaped crystallite ca. 14 nm) produced by forced hydrolysis, at ca. 400 °C for X-ray amorphous microspheres obtained by mixed-solvent precipitation, and at ca. 600 °C for X-ray amorphous powder, obtained by alkoxide hydrolysis and condensation. The formation of tetragonal zirconia is probably related to the presence of amorphous zirconia because of their structural similarity, leading to the possibility of topotactical crystallization on nuclei of amorphous zirconia as a mechanism of crystallization of tetragonal zirconia. This special feature of nanocrystalline materials forms the basis of improvement of stability of thermally grown oxide by nano-controlling.[3]

We observed three kinds of structures with different coalescence within one microfiber located between the heated and unheated zones, Figure 7. The ordering and porosity decreases when going from the "cold" to "hot" part of the microfiber. Remarkably, the nanoparticles remain amorphous after the coalescence in this heating zone, according to the TEM data, Figure 8c. Indeed, the fast Fourier transform (FFT) of the image on Figure 8d shows weak diffraction spots of only photonic crystal but not diffraction due to crystallinity of SiO_2 grains. Diffusion of atoms on the cluster surface toward regions of lower curvature (less strongly bound to the neighboring atoms) was suggested as the driving force of coalescence of crystalline nanoparticles.[22] Conceivably, the coalescence of amorphous nanoparticles in microfibers might proceed along another mechanism. The formation of essentially disordered β-cristobalite structure as the first observable crystalline product of annealing of NCA1 confirms this suggestion.

Microfibers with partially coalesced morphology (Figure 7c) can be used for considering the heat-transport properties of nanomaterials. Opto- and microelectronic devices have to remain within the very narrow temperature range to

(18) Butler, M. A.; Dyson, D. J. *J. Appl. Crystallogr.* **1997**, *30*, 467.
(19) Swainson, I. P.; Dove, M. T. *J. Phys.: Condens. Matter* **1995**, *7*, 1771.
(20) Hatch, D. M.; Ghose, S. *Phys. Chem. Miner.* **1991**, *17*, 554.
(21) Hu, M. Z.-C.; Hunt, R. D.; Payzant, E. A.; Hubbard, C. R. *J. Am. Ceram. Soc.* **1999**, *82*, 2313.
(22) De Hosson, J. T. M.; Palatsas, G.; Vystavel, T.; Koch, S. *JOM* **2004**, *56*, 40.

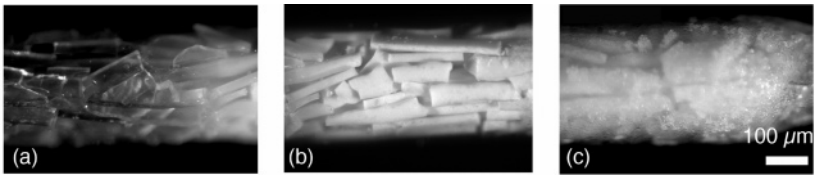

Figure 5. Optical photographs, showing three different zones in the quartz capillary, filled with microfibers M1 (thickness $d = 36$ μm) and studied with in-situ X-ray measurements during heating. (a) Microfibers in the low-temperature zone have a transparency gradient along the crystal length with the opaque part of the crystal in the right (hot) part. (b) Opaque microfibers in the medium-temperature zone. (c) Opaque microfibers and heating products in the high-temperature zone (smaller particles). The X-ray spot size 0.5 mm was focused on this part of the capillary during the in situ X-ray study. Capillary has a diameter of 0.5 mm; wall thickness is 0.01 mm.

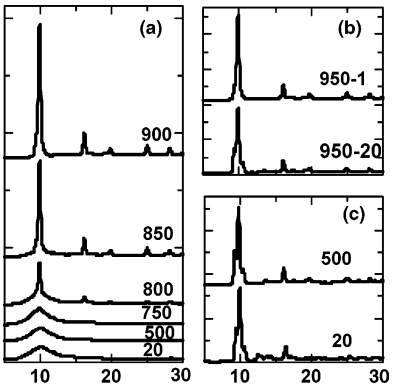

Figure 6. Evolution of X-ray diffraction pattern of the microfibers (thickness $d = 36$ μm) as a function of temperature in the high-temperature zone (final products of annealing are shown on Figure 5c). Duration of every X-ray measurement at constant temperature was 30 min; heating (cooling) rate was 10 °C/min, λ(M*o* Kα1). Three structure transformations of microfibers during the annealing were emphasized. (a) Heating: formation of the β-crystobalite from SiO_2 colloids during the heating at 750−800 °C. (b) Isothermal annealing: formation of the mixture of coexisting cubic β-crystobalite (major phase) and hexagonal tridimite at prolonged isothermal heating at 950 °C during ca. 12 h (pattern 950−20). (c) Cooling: final product contains β-crystobalite, tridimite, and low quartz.

maintain possibility of frequency control, which defines circuit lifetime. This requires efficient directional heat removal. The current leads of high-T_c-superconductors are the opposite example of heat management. They have to have small heat conductivity and need a thermal (e.g., metal oxide) buffer to exclude heat removal. Electronic devices, comprising nano- and/or organic (or biological) components, need especially careful heat management. Thermal conductivity of nanomaterials may differ greatly from microcrystalline materials and depends on the chemical nature of particles, particle size, and particles arrangement (aggregation or formation of nanoarrays). It is known that phonon transport in nano- and micrograin structures has to be reduced due to scattering at the grain boundaries.[23] This is especially the case, when the grain size becomes comparable to the phonon mean free part (MFP) at given temperature, which can be approximated as $l = 5a(T_m/T)$, where a is the lattice constant, T_m is the melting point, and T is the temperature.[24] For SiO_2 (quartz), $l \approx 200$ Å at 300 K. Phonon transport in sintered structures depends on the diameter and transparency of the interface necks.[25] The necks become transparent for phonons, if the neck size becomes comparable to the grain size.[26] The anisotropy of thermal conductivity equals approximately $(k_{||}/k_{\perp}) = (S_{||}d_{\perp}/S_{\perp}d_{||})$, where $k_{||}$, $k_{\perp}$ are heat conductivities along and normal to the array direction, $S_{||}$, $S_{\perp}$ are the neck areas, and $d_{||}$, $d_{\perp}$ are the grain sizes in the directions along and normal to the array direction. This is the situation we observe in sintered SiO_2 microfibers, Figure 7c. By this means, controlled sintering can be used for fabrication of nanodevices with controlled thermal properties of nanoarrays (amount and anisotropy of heat transport).

To get the anisotropic networks of grains, connected through transparent for phonons necks, we have to keep the sintering at the retarded elastic response state.[27] We can then design a structure with an anisotropy of thermal conductivity of corresponding dimensionality. According to the microfiber morphology shown in Figure 7, the gradient of the phonon transport properties with the length of the nanofiber can be also expected, allowing for consideration of the partially sintered nanocrystalline silica microfibers as nanocrystalline graded materials.[28] The measurement of the dependence of the degree of sintering of nanocrystalline microfibers on the temperature is in progress now. A significant and rapid (within less than 1 h) change in the properties of silica nanoparticles (removing water, elimination of pores, shrinkage) is expected already at the temperature 300 °C.[29]

The microfibers after complete coalescence of nanoparticles in the high-temperature zone are very porous but retain perfect shape with a rectangular cross-section, Figure 9a and b. Notice that microfibers subjected to high-temperature treatment are built of crystals with grains size much larger than phonon MFP and can be considered as bulk materials. This concerns phonon transport properties. The presence of uncoalesced nanoparticles on the surface of micrometer-sized β-cristobalite crystals (Figure 9c) after prolonged (around 12 h) heating may indicate the formation of crystalline SiO_2 nanoparticles if coalescence is kinetically hindered.

The nanocrystalline structure, shown in Figure 3a, consisting of nearly parallel micrometer-sized arrays, stabilized by the previously described drying procedure, could be characterized by three levels of organization as follows.

Crystallinity of Constituent SiO_2 Nanoparticles. According to TEM data, primary SiO_2 particles (see Experimental Section) and SiO_2 particles, partially coalesced in the middle heating zone (Figures 5, 7, and 8), are amorphous.

(23) Klemens, P. G.; Gell, M. *Mater. Sci. Eng.* **1998**, *A245*, 143.
(24) Ziman, J. M. *Electrons and Phonons*; Clarendon Press: Oxford, 1960.
(25) Braginsky, L.; Lukzen, N.; Shklover, V.; Hofmann, H. *Phys. Rev. B* **2002**, *66*, 134203.
(26) Braginsky, L.; Shklover, V.; Bowen, P.; Hofmann, H. *Phys. Rev. B* **2004**, *70*, 134201.
(27) Mazur, S.; Beckerbauer, R.; Buckholz, J. *Langmuir* **1997**, *13*, 4287.
(28) Mijamoto, Y.; Kaysser, W. A.; Rabin, B. H.; Kawasaki, A.; Ford, R. G. *Functionally Graded Materials: Design, Processing and Applications*; Kluwer Academic Publishers: Norwell, MA, 1999.
(29) Chabanov, A. A.; Jun, Y.; Norris, D. J. *Appl. Phys. Lett.* **2004**, *84*, 3573.

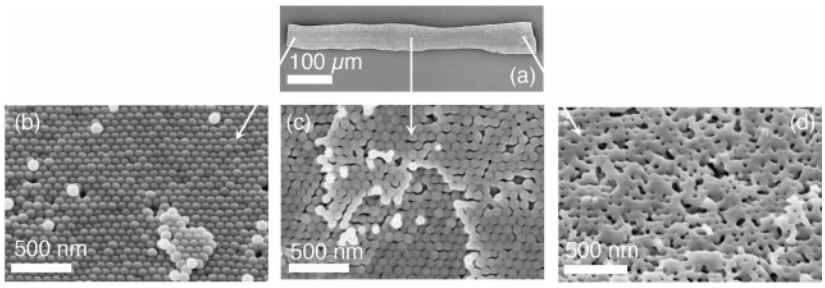

Figure 7. SEM patterns, illustrating structure of the partially transparent microfibers (thickness $d = 36$ μm, low-temperature zone on Figure 4a) as a function of the temperature gradient in the capillary during annealing. (a) Microfiber used for SEM measurements. All of the SEM patterns (b−d) were recorded from this crystal. (b) Ordered closest ccp packing in the "cold" part of the microfiber. (c) Sintered structure in the middle part of the microfiber. The partial coalescence is observed, but the structure still exhibits ordering. (d) Sintered "hot" part of the microfiber with local markers of the ordering still present.

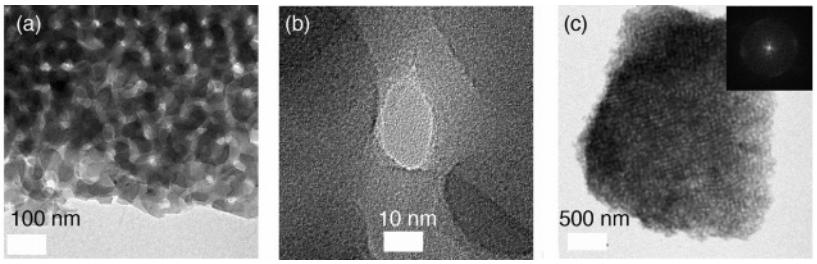

Figure 8. TEM patterns of powderized microfibers (thickness $d = 36$ μm). (a) Partially ordered structure in the middle part of the microfibers. (b) Essentially amorphous structure of the particles and interface "necks" in the middle and "hot" parts of the microfiber. The absence of crystallinity was checked also by recording diffraction patterns. (c) Fragment of the microfiber M2 from the middle part. (Onset) Diffraction due to only the photonic structure of M2 could be seen; there was no diffraction due to crystallinity of SiO_2.

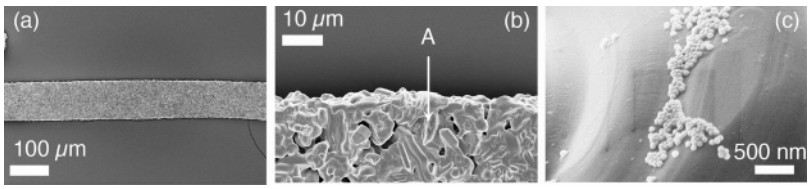

Figure 9. SEM patterns of the microfiber M3 (thickness $d = 36$ μm), consisting of the mixture of β-cristobalite and tridimite. (a,b) Morphology of crystals. (c) Nanocrystals SiO_2, remaining on the surface of sintered micrometer-sized crystals after annealing (A in Figure 9b).

Structure of Self-Assembled Microfibers. The microfibers exhibit the ccp packing of the SiO_2 nanospheres, usual for self-assembled nanocrystalline arrays, with the unit cell constant of the corresponding cubic cell $a = \sqrt{2D} = 113$ nm, the interplanar separation in the direction normal to the substrate surface $d_{111} = \sqrt{2/3D} = 65.3$ nm, and the position of the minimum in transmission spectrum for normal incidence to (111) face as $\lambda_1 = 2d_{111}n_{\text{eff}} \sin \theta = 172.4$ nm (UV range), where refraction index n_{eff} is calculated for a packing density of 0.74 and a refraction index of SiO_2 of 1.46.

Structure of Self-Assembled Film. Parallel microfibers are aligned as one layer into a film. The faces of both microfibers and film have rational crystallographic orientation with regards to the crystallization cell and controlled thickness. Further investigations of the dependence of the morphology of the nanocrystalline microfibers and films on the design of the crystallization cell are in progress.

Conclusion

Using shear-flow crystallization of colloidal particles, ordered microcrystalline arrays of spherical SiO_2 nanoparticles are obtained (microfibers, films). These arrays have a controllable thickness, a distinct crystallographic orientation of external surfaces, and can be described as ccp of spherical particles. The observed rational orientation of exposed crystallographic faces of the microfibers and laminas in the crystallization cell indicates the possibility of monitoring the crystallization process. High-temperature annealing leads to the transformation of low-dimensional colloidal arrays into β-cristobalite structure at 750−800 °C (major product), which further transforms into a mixture of SiO_2 polymorphs at both prolonged heating and cooling. The presence of more disordered β-cristobalite in the annealing product of colloidal nanocrystalline array is remarkable. In the low-temperature zone, the structures with a gradient of morphology (ordering, grain size, porosity) due to temperature gradient along the array length are obtained and characterized. The size of the sintering neck size between the nanoparticles and, by this means, the phonon transport properties in the partially sintered ordered nanocrystalline arrays can be changed. This can be used for monitoring both the amount and the anisotropy of heat transport. The performed study can be considered as a part of the development of a strategy (which could require both self-assembly and template-assisted steps) toward a bottom-up approach to the design of ordered nanostructure arrays.

Acknowledgment. This work has been supported by the TOP NANO 21 program (Swiss Commission for Technical Innovations, project No. 5971.2 TNS). I thank Prof. Y. Xia and Dr. J. McLellan (Department of Chemistry, University of Washington, Seattle) for their hospitality and a kind introduction to the shear-flow crystallization method, and Prof. L. Braginsky (Institute of Semiconductor Physics, Novosibirsk, Russia) for discussions of thermal conductivity in nanostructures. I am also indebted to colleges from the Swiss Federal Institute of Technology (Zürich): Prof. N. D. Spencer (Institute of Surface Science and Technology) for access to laboratory equipment, Prof. L. Gauckler (Institute of Non-Metallic Materials) for access to the SEM microscope LEO 1530, Dr. C. Beeli (Institute of Solid State Physics) for the help in recording TEM patterns, and Dr. G. Krauss (Laboratory of Crystallography) for assistance in high-temperature X-ray measurements with the Mar300 image plate scanner.

Supporting Information Available: Materials used and figures (PDF). This material is available free of charge via the Internet at http://pubs.acs.org.

CM048870T